Fast Online Acquisition and Analysis for Parison Swell and Sag in Blow Molding

Han-Xiong Huang, Jiong-Cheng Li

Center for Polymer Processing Equipment and Intellectualization, College of Industrial Equipment and Control Engineering, South China University of Technology, Guangzhou, People's Republic of China

Received 20 July 2005; accepted 9 November 2005
DOI 10.1002/app.23881
Published online in Wiley InterScience (www.interscience.wiley.com).

ABSTRACT: It is critical to quantitatively and reliably characterize the effects of swell and sag phenomena on the final parison dimensions in extrusion blow molding. To achieve this goal, an online image acquisition and analysis technique was developed. The successive images of parison were automatically taken using the online acquisition apparatus. These images were then analyzed by the combined use of the conventional digital image processing method and the new one developed by the authors. So the development of parison diameter and thickness swells with the extrusion time could be determined online. On the basis of the online obtained actual swell values, the pure swell and sag components were quantitatively determined. The developed technique was tested through a series of experiments using several resins under different processing parameters and die types. Shown in the present article were the results for a converging die under three different die gaps and a high-density polyethylene. Some new phenomena were observed using the proposed technique. The results showed that the technique yields fast and accurate determination of the evolution of diameter, thickness, and length of parison during its extrusion. The technique can be employed as a part of the closed loop control for blow molded part thickness. © 2006 Wiley Periodicals, Inc. J Appl Polym Sci 101: 2399–2406, 2006

Key words: extrusion; imaging; molding; polyethylene (PE); swelling

INTRODUCTION

The quality of extrusion blow molded parts, as well as the economic efficiency of their production depends substantially on their wall thickness distribution. So it is crucial to optimize the thickness distribution of the final part. The part thickness distribution is mainly determined by the dimensions of the parison just prior to its enclosure in the mold, which are influenced by the swell and sag phenomena occurring during the parison extrusion.

The extrusion of the parison out of an annular die and the change in the dimensions of the free standing parison under the combined effects of swell and sag are complicated. Both swell and sag effects are time and temperature dependent. Considerable effort has been put into the mathematical simulation of parison extrusion,[1–5] especially the phenomena of swell and sag. Numerical simulations on the parison extrusion help minimize machine setup times and tooling costs as well as optimize processing parameters to yield desired final part specifications. However, numerical simulations on the swell and sag involve significant simplifications and are quite time-consuming. Moreover, previous study results showed that the predicted extrudate swell values are sensitive to the choice of constitutive equation.[3,4] For example, Otsuki et al.[4] carried out numerical simulations of parison swells extruded through the straight, divergent, and convergent dies. Several important viscoelastic models, the K-BKZ, the PTT, and the Larson models, which can express well the shear flow characteristics of high-density polyethylene (HDPE), were used. Their studies demonstrated that there are remarkable differences among the results of these viscoelastic models. Recent study by Huang et al.[6] also showed that some difference exists between the numerical prediction and the experimental data of parison diameter and thickness swells. The extent of difference is affected by the values of the material parameters in the Wagner damping function when choosing the K-BKZ constitutive equation. So accurate numerical prediction of the parison swell and sag is quite difficult.

Experimental techniques are efficient to determine both transient and final swell and sag behaviors of the parison. Several techniques have been proposed to measure the parison diameter and thickness distribu-

Correspondence to: H.-X. Huang (mmhuang@scut.edu.cn).
Contract grant sponsor: National Natural Science Foundation of China; contract grant number: 50390096.
Contract grant sponsor: Major Project of Key Fields in Guangdong-Hongkong; contract grant number: 2004A10402003.
Contract grant sponsor: Teaching and Research Award Program for Outstanding Young Teachers in Higher Education Institutions of MOE, People's Republic of China.

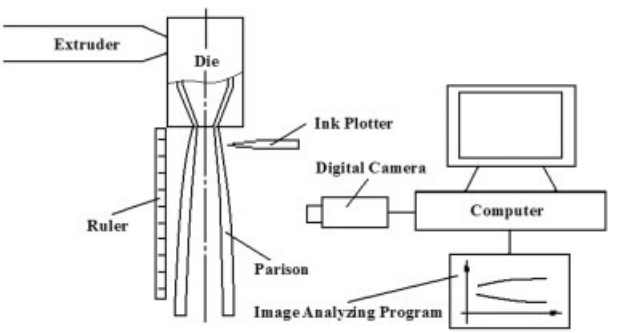

Figure 1 Schematic of the experimental equipment.

tions online.[7–11] More recently, on the basis of a series of online-obtained experimental data, Huang et al.[10,12,13] utilized the neural network method to predict the diameter and thickness swells of the parison. The results showed that the combined use of the experiments and the neural network method can predict the parison swells with a high degree of precision. The advantages of employing the neural network method over simulations based on numerical techniques include the following: (1) no or a minimal number of simplifying assumptions; (2) no need for constitutive equations, and thus no need for difficult-to-obtain rheological data; (3) online prediction for process monitoring and control; and (4) Faster response.

To realize online process monitoring and control by combining the neural network method with experiments, two requisites must be met. First, the parison dimensions must be fast and accurately determined online. The experimental measuring techniques have to be further developed to quantitatively and reliably characterize the effects of both swell and sag phenomena on the final parison dimensions, including the diameter and thickness. Second, some further modifications must be carried out to speed up the algorithm of neural network model. This work aims to present a new, fast, and accurate analysis technique for determining the swell and sag behaviors of the parison directly on an industrial blow molding machine.

Online acquisition of parison images

The experimental equipment employed in the present work is schematically shown in Figure 1. It consisted of an industrial extrusion blow molding machine and an online acquisition apparatus. The extruder used had a screw diameter of 55 mm and a length-diameter-ratio of 25 : 1. The online acquisition apparatus used to take the parison images mainly included a digital camera and a personal computer. The digital camera, with 5 megapixel, was mounted perpendicular to the axis of the parison. After cutting the parison at the die exit at time "zero," the successive images of the parison were taken automatically by the digital camera at 2 fps. During the extrusion of the parison, ink marks were put on its outer surface just below the die exit at the same time interval. The time between the adjacent two ink marks was about 1.0–1.5 s depending on the extrusion flow rate.

The acquired parison images were then sent to the hard disk of the personal computer and were processed. Figure 2 shows typical parison images taken at a sequent time. The corresponding time when the parison reached some length could be determined by analyzing the images.

Online analysis for parison dimension distributions

Two swell values, a diameter swell and a thickness swell, are required to describe the parison dimensions. So the target of the online analysis of parison images is to detect the outer boundaries of the parison and the

Figure 2 Typical parison images taken at a sequent time.

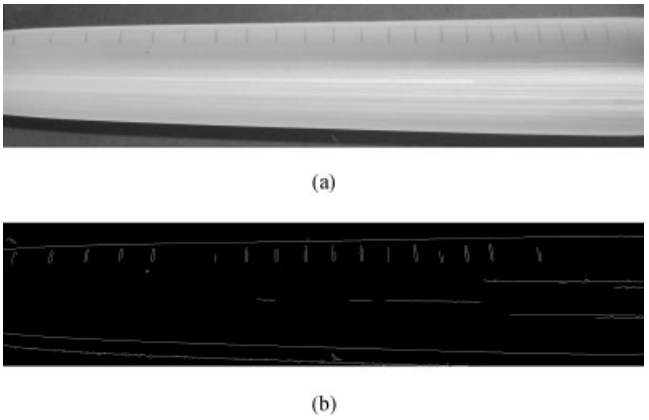

Figure 3 (a) A parison with ink marks and (b) detection results for it using "canny" method.

ink marks on it to determine the outer diameter corresponding to each mark and the distance between adjacent two ink marks. Then the parison thickness corresponding to each mark could be calculated based on the mass conservation.

Edge detection

Many methods on digital image processing technology have been developed for edge detection.[14] All these methods look for the places in the image where the intensity changes rapidly on the basis of derivative estimators. In general, they determine whether a pixel is at edges according to two criteria: the first derivative of the intensity is larger in magnitude than certain threshold, or the second derivative of the intensity has a zero crossing. The Sobel and Canny methods are the most important two. The two methods are provided in the image processing toolbox of Matlab 7.0. Having done many trials, the Canny method, which was developed by Canny,[15] was found to be more suitable for the edge detection of parison than the Sobel method in this work. So the Canny method was adopted. In this method, detection and localization criteria were defined for edge detection and a third criterion was added to ensure that the detector has only one response to a single edge.

Figure 3b shows the detection results for the parison shown in Figure 3a using the Canny method. As can be seen from Figure 3b, the outer boundaries of the parison and some ink marks on it were detected. Similar results were obtained using the other conventional edge detection methods. The detection results of marks on the parison were obviously unsatisfactory. Using the conventional methods, only some points at the edge of marks were detected [as shown in Fig. 3(b)], but the exact position of marks could not be determined.

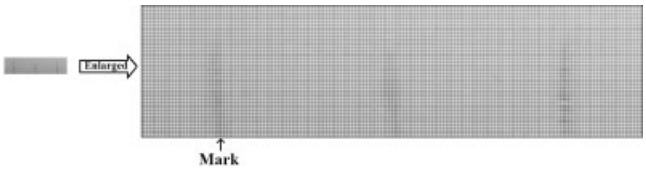

Figure 4 Enlarged local image with marks on the parison.

Mark detection

Consequently, a new method has to be developed to detect the ink marks on the parison. After many efforts were done by authors, a statistic method based on the mean intensity value of each column of pixel was developed. In fact, it can be seen that a digital image consists of a matrix of pixels when it is enlarged. Figure 4 shows an enlarged local image with marks on the parison. There exists an intensity value corresponding to every pixel of the matrix. The range of the intensity value is from 0 to 255. The lighter the pixel is, the larger the intensity value is. The intensity values of white and black pixels are 255 and 0, respectively. The mean intensity value corresponding to each column of pixels could be calculated, which was shown in Figure 5. In this figure, the abscissa is the number of the column in the matrix, or the number of pixels. The mean intensity for the columns of the pixels corresponding to the ink marks on the parison is smaller because the marks are darker. As shown in Figure 5, there exists an exact "valley" corresponding to each ink mark on the parison image. All the columns of the pixels in a valley can be easily located. The column corresponding to the minimum mean intensity in a

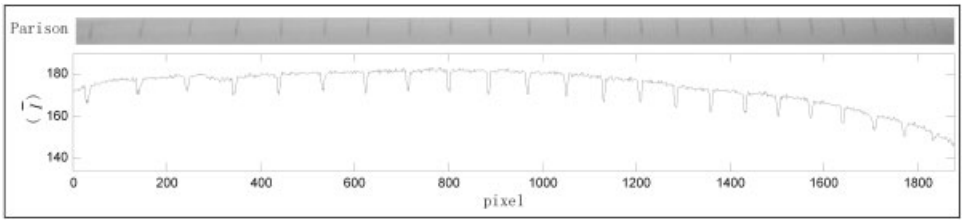

Figure 5 Mean intensity profile ($\bar{I}$) corresponding to each column of pixel on the parison image.

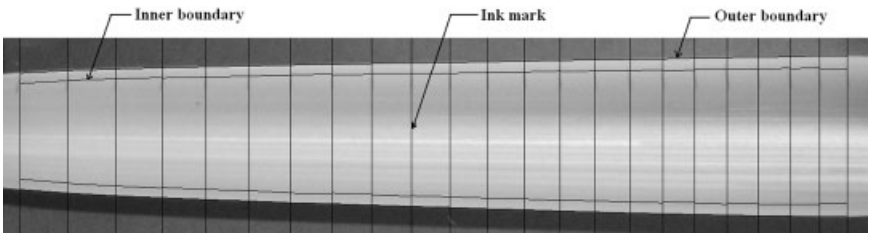

Figure 6 Parison covered with the corresponding detection results.

valley is the position of the bottom of the valley, or the position of the corresponding ink mark.

The new method proposed in this work can work better than the conventional ones. Only the calculation of the mean intensity value of each column of pixels is required for the new method, but the calculation of square, square root, and numerical derivative is required for the conventional methods. As a result, the computer time for the former is much less than that for the latter.

To check the precision of the new method, the parison was covered with the corresponding detection results, as shown in Figure 6. It is shown that the outer boundaries of the parison and all ink marks on it were exactly detected by combining the conventional digital image processing method with the new one developed by the authors.

Parison thickness calculation

The parison segment between adjacent two ink marks was assumed as a tapered cylindrical symmetry with a constant thickness, as shown in Figure 7. Set the nearest ink mark from the die exit at M_0, the second nearest one at M_1, and so on. The outer diameter of the annulus corresponding to M_i was denoted by D_i. The thickness, distance, and volume of the parison segment between marks M_i and M_{i+1} were denoted by H_i, Δl_i, and V_i, respectively. The V_i can be calculated by

$$V_i = \pi \Delta l_i \left(\left[\frac{D_{i+1}}{2} - H_i \right) + \frac{D_i}{2} \right] H_i \quad (1)$$

According to the relationship between mass and volume, the V_i can also be calculated by

$$V_i = \frac{Q \Delta t}{\rho} \quad (2)$$

where Q is the extrusion mass flow rate, Δt the time between two adjacent ink marks, and ρ the melt density of the material used.

Combining eqs. (1) and (2) results in

$$H_i = \frac{(D_{i+1} + D_i)}{4} - \sqrt{\left(\frac{D_{i+1} + D_i}{4} \right)^2 - \frac{Q \Delta t}{\rho \Delta l_i \pi}} \quad (3)$$

By processing the parison images mentioned earlier, the D_i, D_{i+1}, and Δl_i were obtained. Then the H_i could be calculated from eq. (3). After calculating the thickness along the parison, its inner boundaries could be determined, as shown in Figure 6.

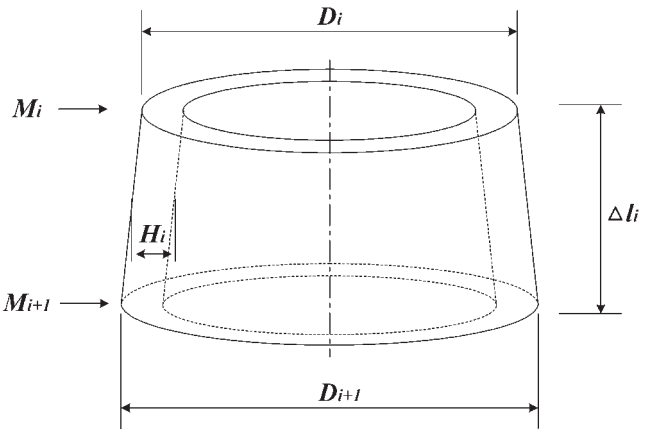

Figure 7 Schematic of approximating a parison segment using a tapered cylinder geometry with a constant thickness.

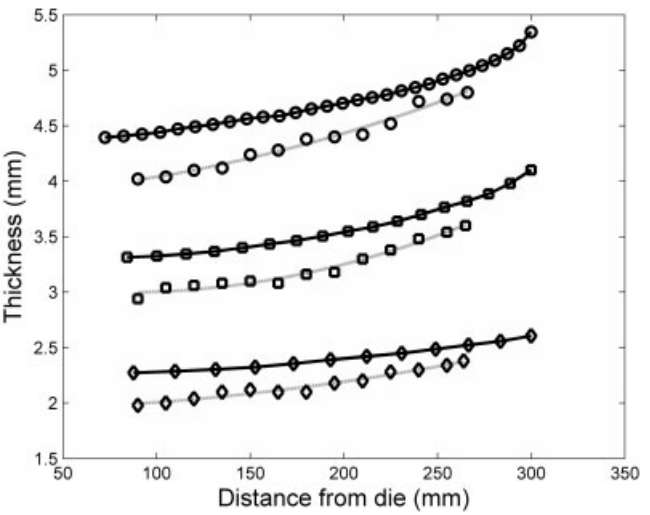

Figure 8 Parison thickness profile comparison between online (——) and offline (----) measurement for (○) 80%, (□) 50%, and (◇) 20% die gap opening.

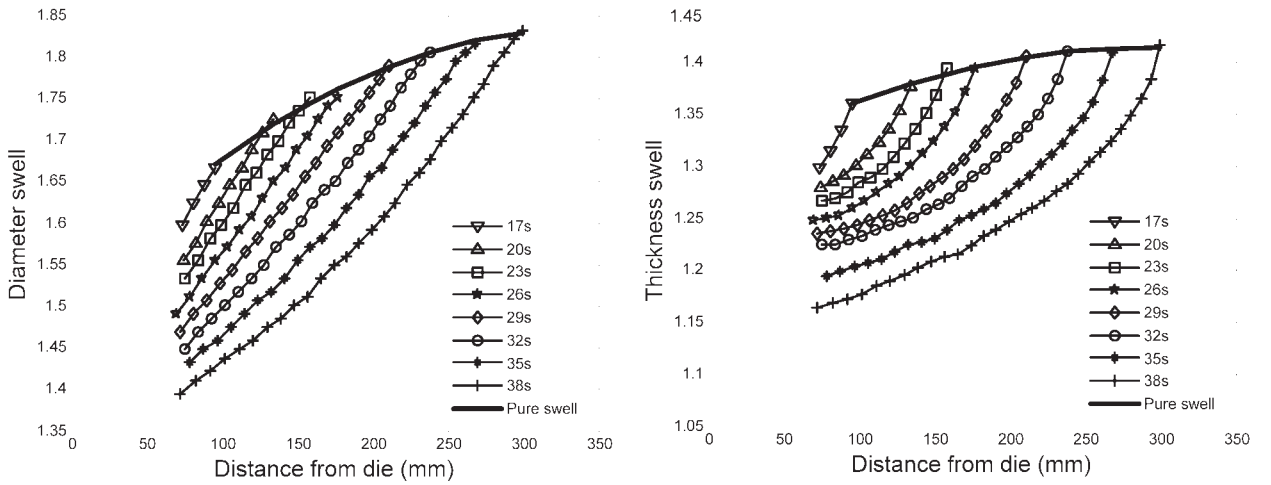

(a)

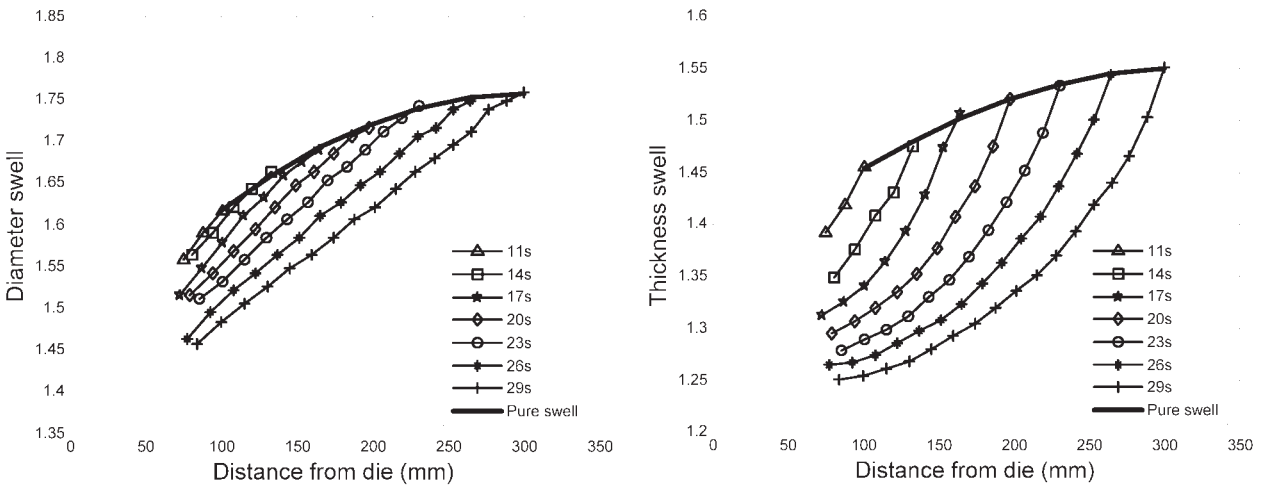

(b)

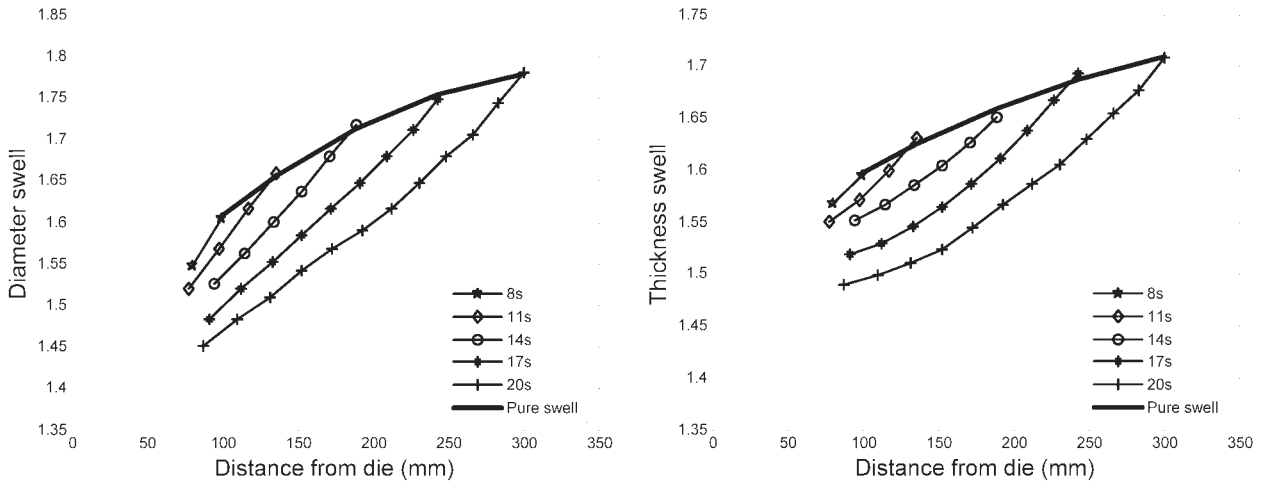

(c)

Figure 9 Online determined evolution of the diameter and thickness swells of the parison with its extrusion time for different die gap openings (%): (a) 80; (b) 50; (c) 20.

Therefore, by analyzing each image sequence of the parison, its diameter and thickness swells could be determined.

RESULTS AND DISCUSSION

A series of experiments were carried out using several high-density polyethylene (HDPE) resins under different processing parameters (extrusion flow rate and melt temperature) and die types (straight, converging, and diverging types) to test the technique developed in this work. Shown here were the results for the HDPE 5300B manufactured by Petrochina Daqing Petrochemical Co. This HDPE is an extrusion blow molding grade resin with a melt index of 0.41 g/10 min and a solid density of 0.952 g/cm^3. The parison was extruded through a converging annular die with an outer diameter of 30 mm. The die temperature was set at 200°C. The screw speed was 10.3 rpm and resulting extrusion flow rate was about 13.9 kg/h. During the extrusion of the parison with a total length of about 300 mm, its images were acquired successively.

Parison thickness comparison between online and offline measurements

After each acquisition of parison images, the parison was cooled in water and then cut open. The thickness was measured with a vernier calipers on the solidified parison at some points and compared with that obtained using the online technique. This comparison is illustrated in Figure 8.

In Figure 8, the 50% die gap opening means that the mandrel and die are at the same vertical position. The die gap is 2.50 mm in this case. The 80 and 20% die gap openings mean that the mandrel is above and below the die, respectively. The corresponding die gaps are 3.77 and 1.53 mm in these two cases, respectively. It can be clearly seen from Figure 8 that both length and thickness measured on the cooled parison are smaller than those obtained online from the corresponding parison. This is because the cooling leads to an increase in the material crystallinity and also an increase in the material density. However, the varying trend of the thickness and its value obtained online are in reasonably good agreement with those measured on the solidified parison.

Parison diameter and thickness swells

Using the technique developed in the present work, an immediate calculation of the diameter and thickness distributions of the parison can be carried out as a function of its extrusion time or length at the end of its formation stage. Figure 9 presents the diameter and thickness swells of the parison extruded from the converging die with three different die gap openings. As

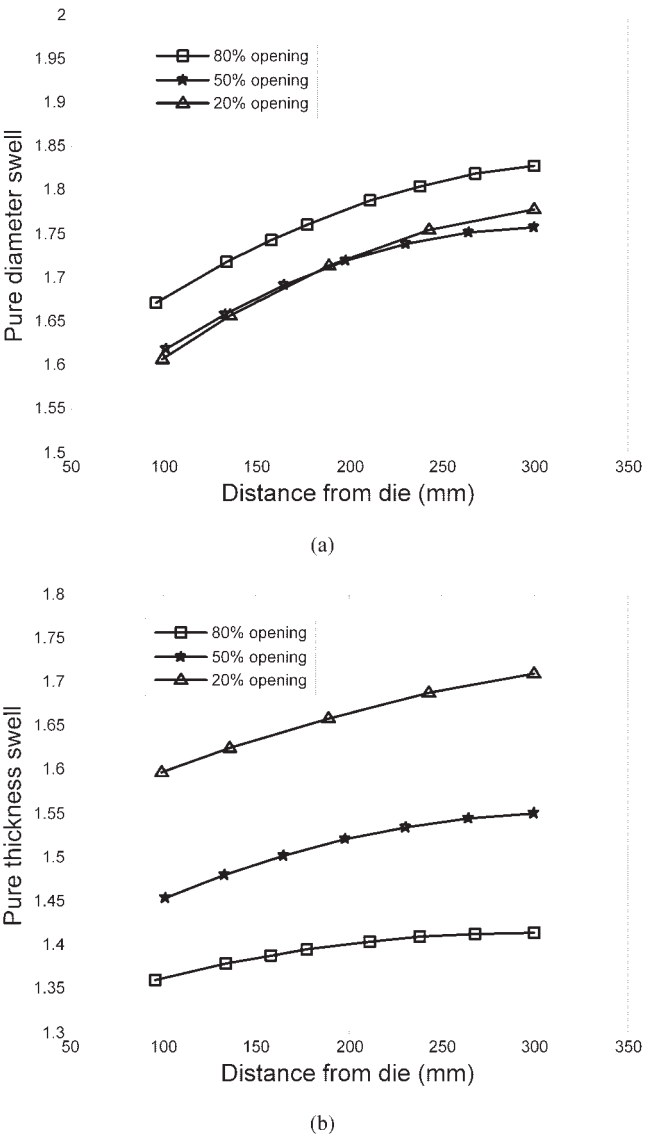

Figure 10 Online determined pure (a) diameter and (b) thickness swells of the parison for different die gap openings.

can be seen, the die gap opening has a little effect on the diameter swell. The thickness swell increases gradually with the decrease of the die gap opening. This can be explained as follows. The thickness swell of the parison is primarily affected by the molecular orientation occurring because of the shear and extensional stresses imposed on the polymer melt during its flow within the extrusion die. The smaller die gap opening results in more rapidly converging streamlines, greater shear and extensional stresses, enhanced molecular orientation, and consequently a larger thickness swell. It can be also seen from Figure 9 that there exists a steep increase of diameter and thickness swells near the die exit. Moreover, the swells at the same distance from the die exit decrease gradually with the increase in the parison extrusion time or its length because of the action of sag.

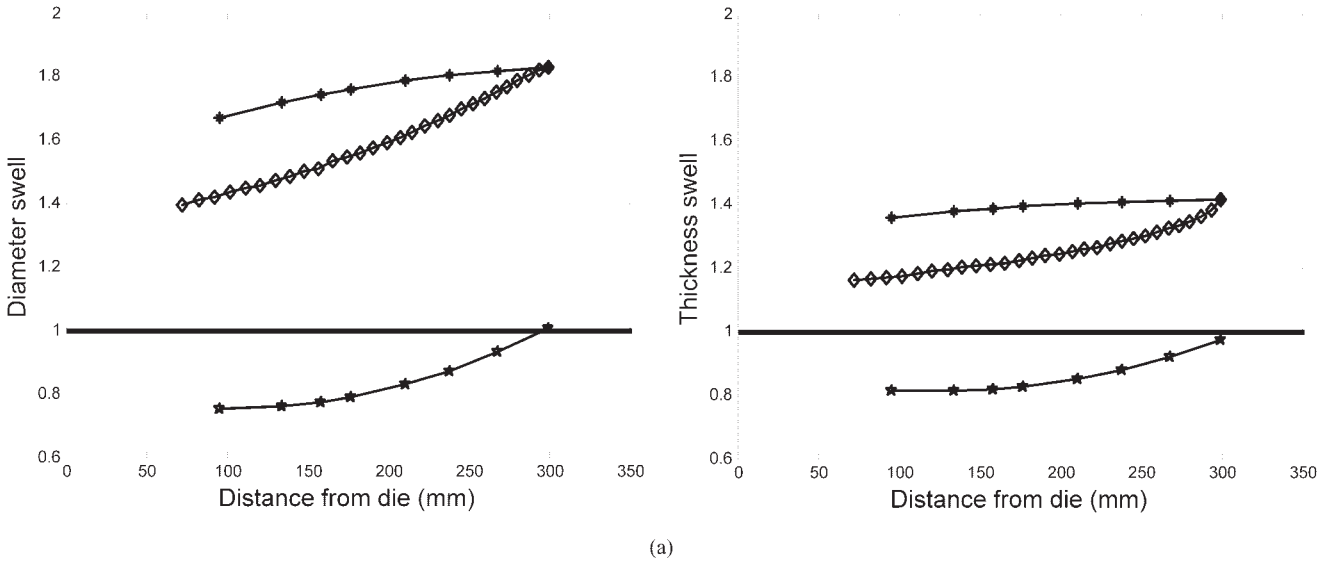

(a)

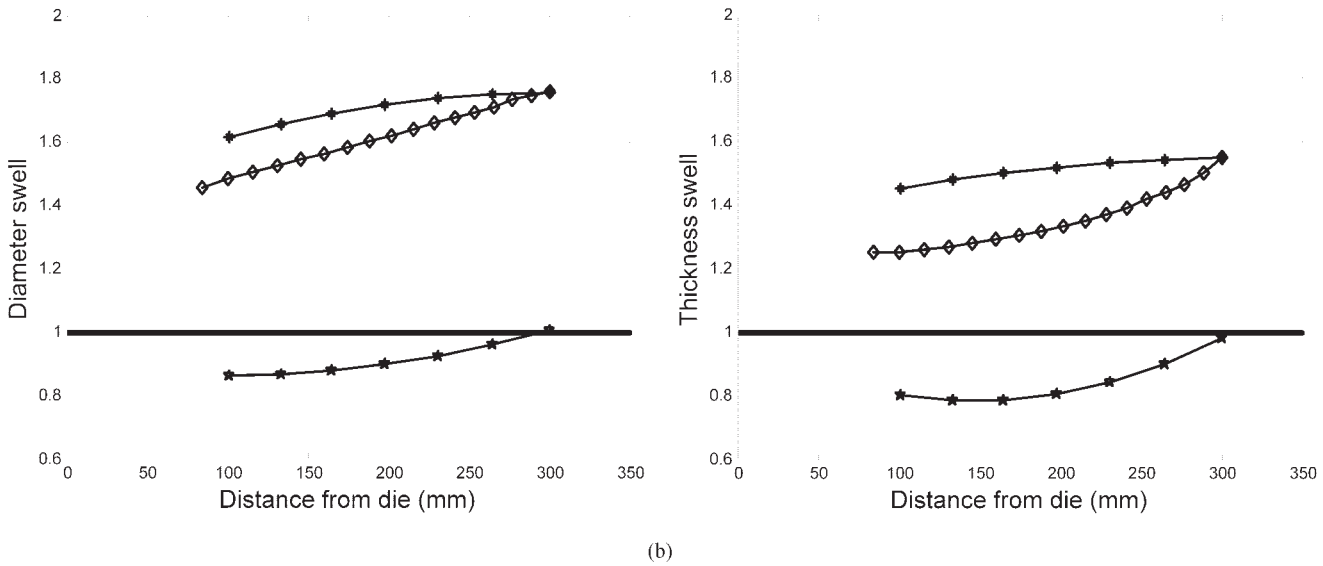

(b)

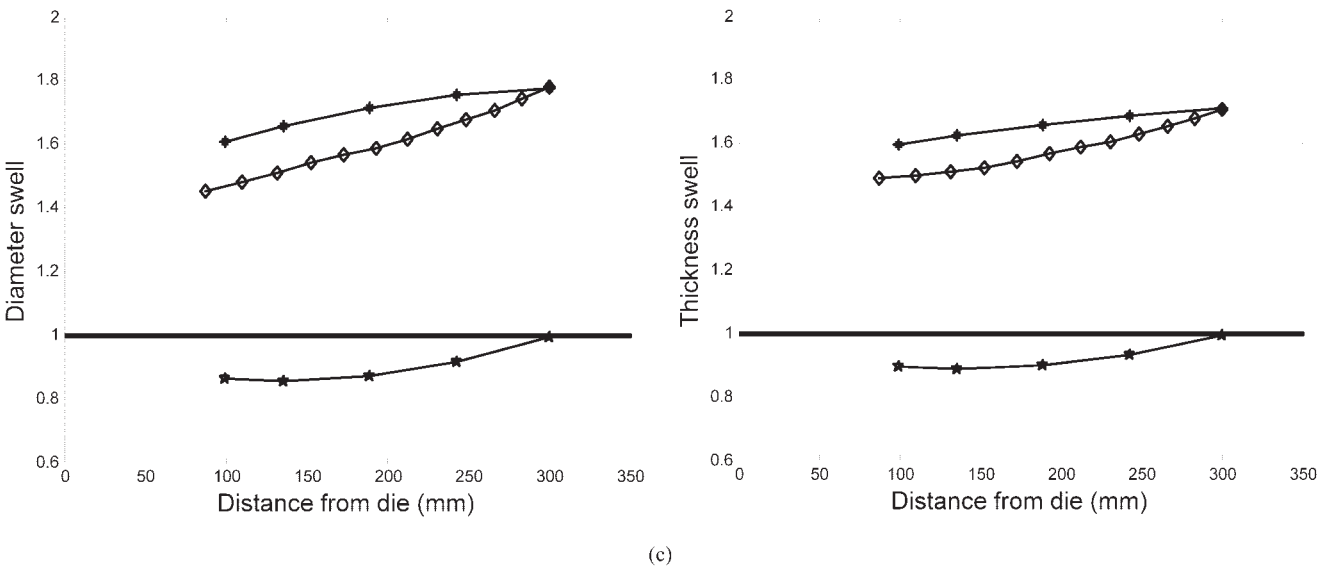

(c)

Figure 11 Decomposition of the swell and sag of the parison for different die gap openings (%): (a) 80; (b) 50; (c) 20. (◇) Actual swell; (+) pure swell; (⋆) pure sag.

It is possible to assume that no sag exists at the extreme bottom of the parison, since there is no weight below it to cause drawdown. Therefore, by fitting the swell values of the bottom of the parison with various lengths, the pure swell curves can be obtained, as shown in Figures 9 and 10. From Figure 10, it is evident that the die gap opening has a smaller effect on the pure diameter swell but a greater effect on the pure thickness swell. The largest pure diameter swell occurs with the 80% die gap opening. This may be attributed to that the extrusion time of the parison is the longest and so it has the most time to achieve a maximum swell in this case. The pure thickness swell increases with the decrease in the die gap opening due to the same reason mentioned earlier. Moreover, the pure swells increase with the parison length, first in a faster rate and then a slower one. After the parison exceeds a certain length, the pure swells tend to plateau values, that is, the ultimate swells. As shown in Figure 10, the pure thickness swell approaches the ultimate swell earlier than the pure diameter swell.

Decomposition of swell and sag phenomena

On the basis of analyzing the pure swells, the contributions of swell and sag phenomena to the final parison dimensions, including the diameter and thickness, can be independently quantified. The effects of swell and sag on the parison dimension distributions along its length can be considered to be additive. Swell and sag phenomena lead to an increase and a decrease of the parison dimensions, respectively. So the pure sag curve can be determined by the difference between the pure swell and the actual swell obtained online under the effect of the sag.

Figure 11 compares the decomposition of the swell and sag for the parison emerging from the die with three different die gap openings. It can be seen that compared with the swell component, the sag one is very small and so has only slight contribution to the parison diameter and thickness for the used material and extruded parison length in this work. The magnitude of the sag slightly increases with increase in the die gap opening because of longer extrusion time and larger weight of the parison.

Using the technique developed in this work, about only 8 s of total time is required for analyzing the successive parison images obtained at one condition to give the diameter and thickness swell evolution (shown in Fig. 9) and decompose the pure swell and sag components (shown in Fig. 11). The technique can work online during the parison formation on any industrial extrusion blow molding machine and assist the operators to quantitatively analyze the effects of the swell and sag on the parison dimensions. So less time and resin are needed to start the blow molding process. The developed technique is useful for designing the blow molding resins by establishing the relationship between polymer molecular structure and both swell and sag behaviors of the parison. The ability of fast and accurate online determination of parison dimensions should prove to be helpful to investigate the swell and sag behaviors of different resins under different processing parameters and die designs, develop the improved models for the parison formation, and to take proper action to optimize a given blow molding operation. More importantly, the proposed technique can be employed as a part of a closed loop control for the final blow molded part thickness distribution.

CONCLUSIONS

Both swell and sag influence the diameter and thickness of the parison in extrusion blow molding process. An online acquisition apparatus was used to automatically take the successive images of the parison during its extrusion from a commercial extrusion blow molding machine. By analyzing these images by combining the conventional digital image processing method with the new one developed by the authors, the evolution of the parison diameter and thickness swells with its extrusion time or length could be fast determined online. Swell and sag contributions to the final parison dimensions were then decomposed.

Results obtained with this technique were presented for a converging parison die under three different die gap openings and a high-density polyethylene (HDPE) resin. The results showed that the diameter swell changes little but the thickness swell increases gradually with the decrease in the die gap opening. For the HDPE used in this work, the sag component is very small when compared with the swell one. On the basis of the results, the swell and sag of the parison can be kept under control by adjusting the die gap opening.

References

1. Seo, Y. J Appl Polym Sci 1990, 41, 25.
2. Tanoue, S.; Iemoto, Y. Polym Eng Sci 1999, 39, 2172.
3. Garcia-Rejon, A.; DiRaddo, R. W.; Ryan, M. E. J Non-Newtonian Fluid Mech 1995, 60, 107.
4. Otsuki, Y.; Kajiwara, T.; Funatsu, K. Polym Eng Sci 1999, 39, 1969.
5. Tanifuji, S. I.; Kikuchi, T.; Takimoto, J. I.; Koyama, K. Polym Eng Sci 2000, 40, 1878.
6. Huang, H. X.; Miao, Y.S. ASME J Fluids Eng, to appear
7. DiRaddo, R. W.; Garcia-Rejon, A. Polym Eng Sci 1992, 32, 1401.
8. Eggen, S.; Sommerfeldt, A. Polym Eng Sci 1996, 36, 336.
9. Swan, P. L.; Kamal, M. R.; Garcia-Rejon, A.; Cielo, P. Polym Eng Sci 1996, 36, 985.
10. Huang, H. X.; Liao, C. M. Polym Test 2002, 21, 745.
11. Stéphenne, V.; Pestiaux, P.; Maziers, E. Paper presented at the Proceedings of Annual meeting of Polymer Processing Society 2004, Akron, OH. Paper 416.
12. Huang, H. X.; Lu, S. J Appl Polym Sci 2005, 96, 2230.
13. Huang, H. X.; Lu, S. J Reinforc Plast Compos 2005, 24, 1025.
14. Gonzalez, C. R.; Woods, R. E. Digital Image Processing, 2nd ed.; Prentice Hall: New Jersey, 2002.
15. Canny, J. IEEE Trans Pattern Anal Mach Intell 1986, 6, 679.